

Ultra-Thin Hematite on Mesoporous WO₃ from Atomic Layer Deposition for Minimal Charge Recombination

Eunsoo Kim^{a,†}, Sungsoon Kim^{b,†}, Young Moon Cho^b, Jong Hyeok Park^{b,}, and*

Hyunjung Shin^{a,}*

^a *Department of Energy Science, Sungkyunkwan University, Suwon 440-746, Korea*

^b *Department of Chemical and Biomolecular Engineering, Yonsei University, Seoul 120-749, Republic of Korea*

*Corresponding authors

E-mail address: lutts@gmail.com (J. H. Park) & hshin@skku.edu (H. Shin)

KEYWORDS Photoelectrochemical water splitting, Atomic layer deposition, Minimal

charge recombination, Heterojunction interface

Number of pages: 23

Number of figures: 17

Number of tables: 3

Table S1. Fitting results from XRR analysis of ALD grown α -Fe₂O₃ layer. 800 cycle ALD on the Si wafer was used for the measurement.

Material	Thickness (nm)	Density (g/cm ³)	Roughness (nm)
α -Fe ₂ O ₃	16.319	5.498	1.037
SiO ₂	7.51	1.56	0.259
Si (sub.)	-	2.33	1.40

Table S2. Fitting results from Nyquist plot of Fe₂O₃, *m*-WO₃/Fe₂O₃ and *m*-WO₃/Fe₂O₃/TiO₂/CoPi photoanodes

	R _S (Ω)	R _{Bulk} (Ω)	R _{CT} (Ω)
Fe ₂ O ₃	31	177	10,760
<i>m</i> -WO ₃ /Fe ₂ O ₃	42	60	2,729
<i>m</i> -WO ₃ /Fe ₂ O ₃ /TiO ₂ /CoPi	18	24	570

Table S3. Summary of recent reports on WO_3 and $\alpha\text{-Fe}_2\text{O}_3$ heterojunction photoanode for PEC water splitting.

Photoanode	Electrolyte	Photocurrent @ 1.23 V vs RHE (mA cm ⁻²)	Photocurrent @ 1.6 V vs RHE (mA cm ⁻²)	Stability (min)	Ref
$m\text{-WO}_3/\text{Fe}_2\text{O}_3/\text{TiO}_2/\text{CoPi}$	1.0 M NaOH	1.5	4.0	100	Our work
Host/guest F:SnO ₂ /WO ₃ /Fe ₂ O ₃	1.0 M NaOH	1.71	2.0 [#]	-	(22)
WO ₃ NNs/ $\alpha\text{-Fe}_2\text{O}_3$ /Co-Pi	0.1 M KH ₂ PO ₄ /K ₂ HPO ₄	1.8 [#]	2.1	60	(S1)
Fe ₂ O ₃ /WO ₃ NRs	0.1 M Na ₂ SO ₄	1.0	1.3	-	(S2)
FeWONSSs	0.5 M Na ₂ SO ₄	1.66	3.3 [#]	600	(S3)
WO ₃ / $\alpha\text{-Fe}_2\text{O}_3$ /CoPd	0.1 M KP _i	0.5	-	2.5	(S4)
$m\text{WO}_3/\text{Fe}_2\text{O}_3/\text{WO}_3$	0.1 M NaOH	0.7	0.97 [#]	-	(S5)
Bilayer WO ₃ /Fe ₂ O ₃	0.5 M Na ₂ SO ₄	1.25	-	-	(S6)
WO ₃ /Fe ₂ O ₃ /LDH	1.0 M NaOH	0.4 [#]	1.5 [#]	5	(46)
WO ₃ /Ti-Fe ₂ O ₃	1.0 M KOH	2.15	2.5 [#]	117	(S7)
WO ₃ @ $\alpha\text{-Fe}_2\text{O}_3/\text{FeOOH}$	0.2 M Na ₂ SO ₄	1.12	-	5	(S8)
FTO-WO ₃ /Fe ₂ O ₃	1.0 M NaOH	0.05 [#]	0.5 [#]	17	(S9)

[#] Approximately calculated from data

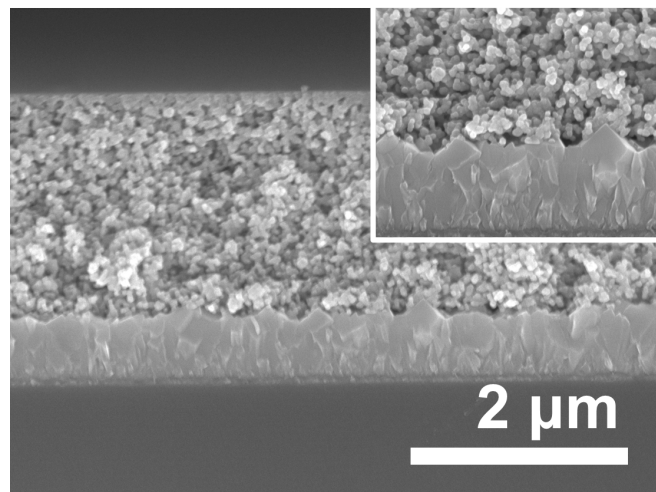


Figure S1. Cross-sectional SEM image of the *m*-WO₃ layer before α -Fe₂O₃ deposition. The inset image shows the interface between the *m*-WO₃ layer and the FTO surface.

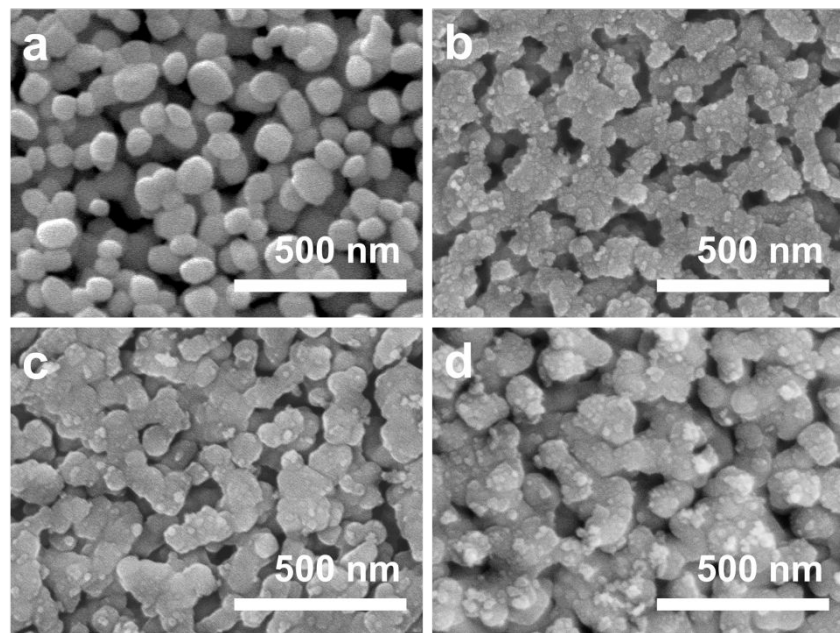


Figure S2. SEM images showing different morphologies of the top surface of each photoanode as the number of ALD cycles increased. (a) $m\text{-WO}_3$ photoanode on a FTO substrate before the ALD process. Photoanodes after different numbers of the ALD cyclic process: (b) 100 cycles, (c) 400 cycles, and (d) 800 cycles. Each $\alpha\text{-Fe}_2\text{O}_3$ layer was postannealed after the ALD process.

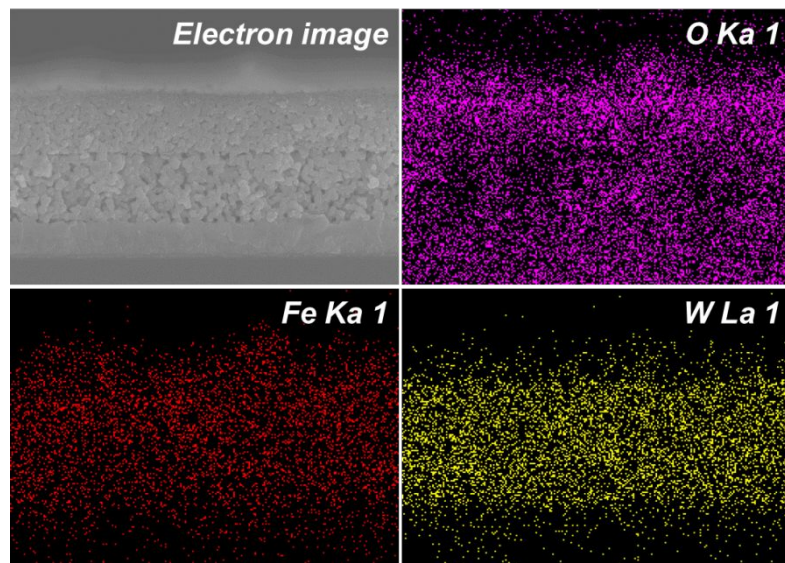


Figure S3. Elemental mapping images of m-WO₃/Fe₂O₃ photoanode with cross-sectional view.

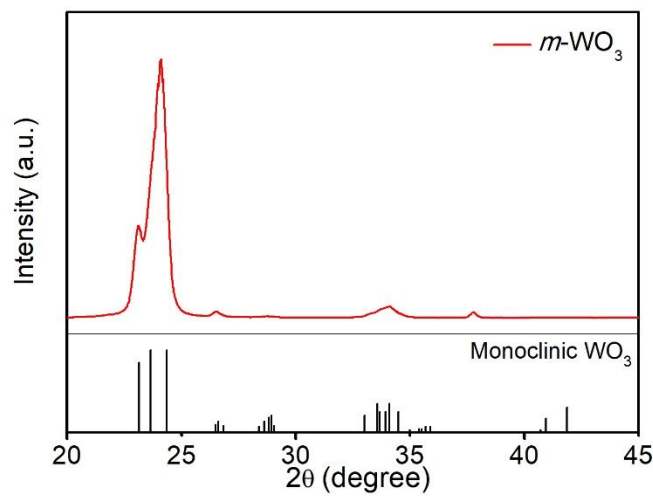


Figure S4. XRD diffraction pattern of $m\text{-WO}_3$ film fabricated by suggested PEG assisted sol-gel process. Reference peak positions and intensities of monoclinic phase are denoted below. Major peak positions of FTO substrate are denoted by the triangle markers.

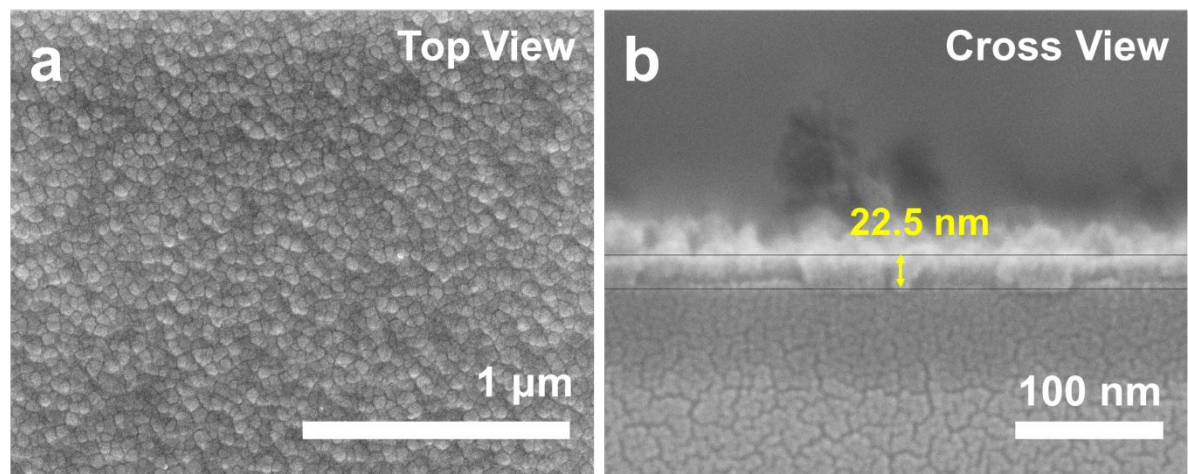


Figure S5. SEM image of α -Fe₂O₃ thin film grown on Si wafer: (a) top view and (b) cross view. The α -Fe₂O₃ was deposited by 800 cycle of ALD process without any *m*-WO₃ scaffold.

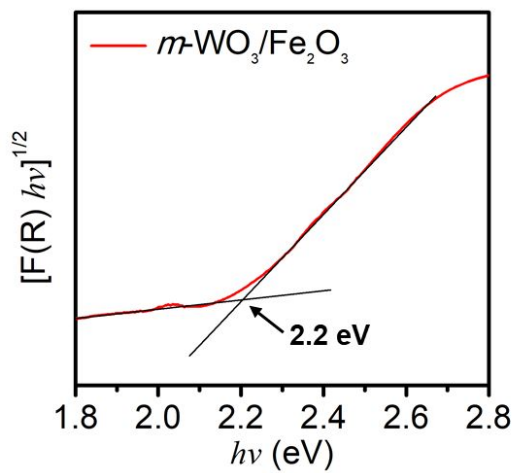


Figure S6. Kubelka-Munk plot of $m\text{-WO}_3/\text{Fe}_2\text{O}_3$ photoanode. The band gap energy was calculated from the intercept between two linearly fitted lines due to the n-type electronic configure of $\alpha\text{-Fe}_2\text{O}_3$ material.

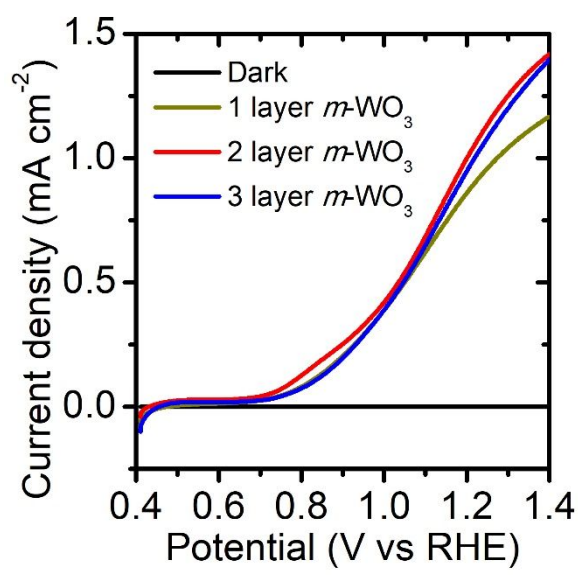


Figure S7. Photocurrent measurement of $m\text{-WO}_3$ photoanode with different number of layers.

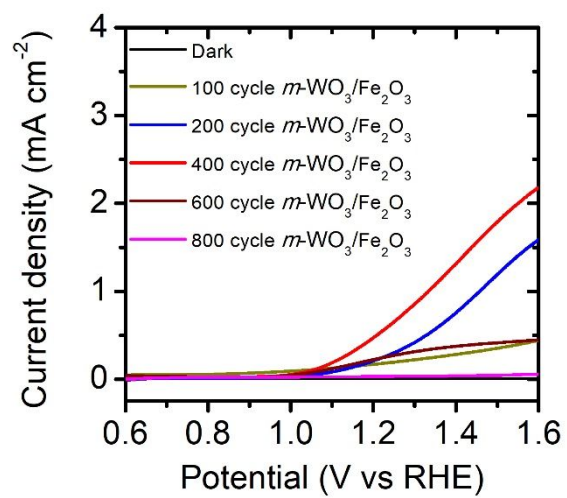


Figure S8. Photocurrent measurement of $m\text{-WO}_3/\text{Fe}_2\text{O}_3$ photoanodes with different ALD cycles. All photoanodes were postannealed after ALD cycles at 500 °C

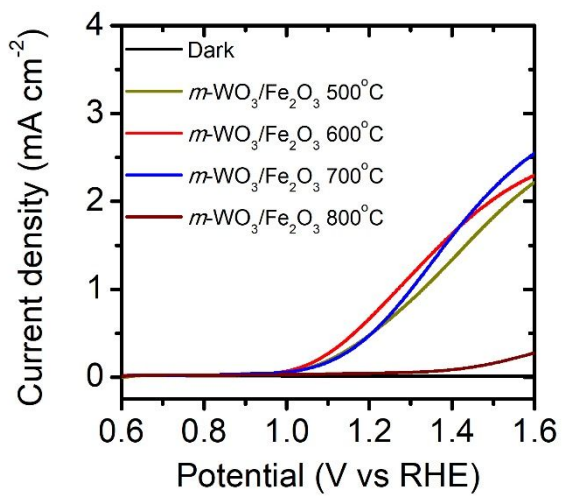


Figure S9. Photocurrent measurement of $m\text{-WO}_3/\text{Fe}_2\text{O}_3$ photoanode with different temperature of thermal treatment from 500 °C to 800 °C. It shows the highest photocurrent of about 0.8 mA/cm^2 at 1.23V vs RHE without any cocatalysts when the cell was treated at 600 °C.

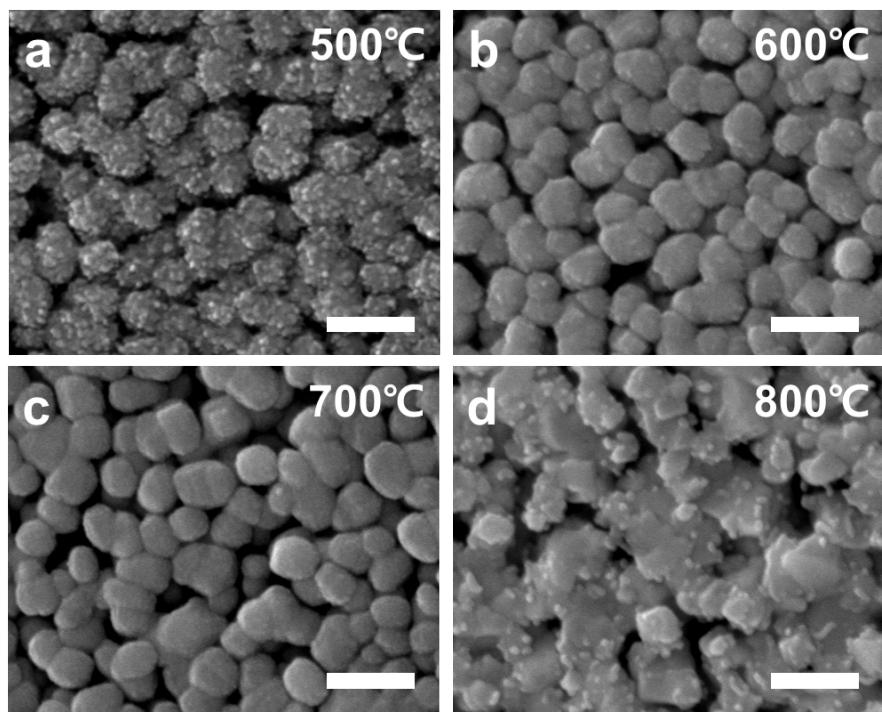


Figure S10. SEM images of 400 cycle m -WO₃/Fe₂O₃ photoanode with different temperature annealing of (a) 500 °C, (b) 600 °C, (c) 700 °C and (d) 800 °C. Scale bars: 200 nm

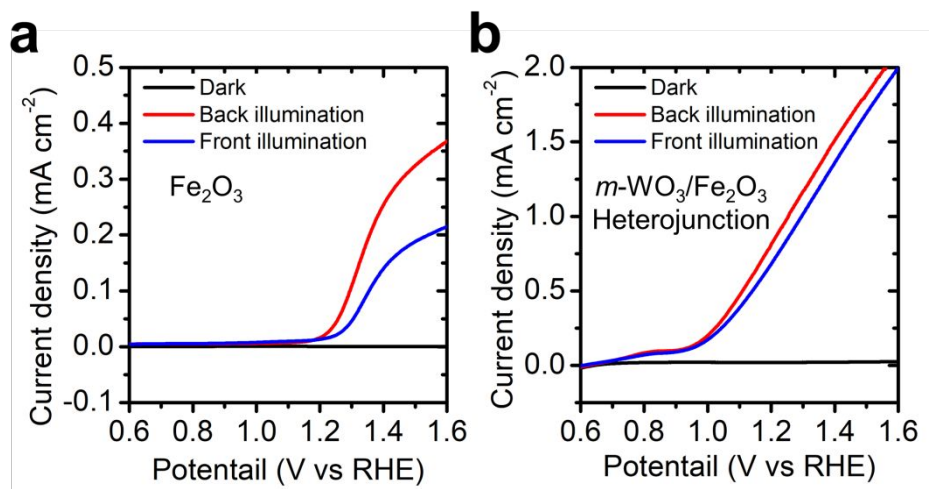


Figure S11. Photocurrent measurement of (a) Fe_2O_3 and (b) $m\text{-WO}_3/\text{Fe}_2\text{O}_3$ photoanodes with different direction of light irradiation.

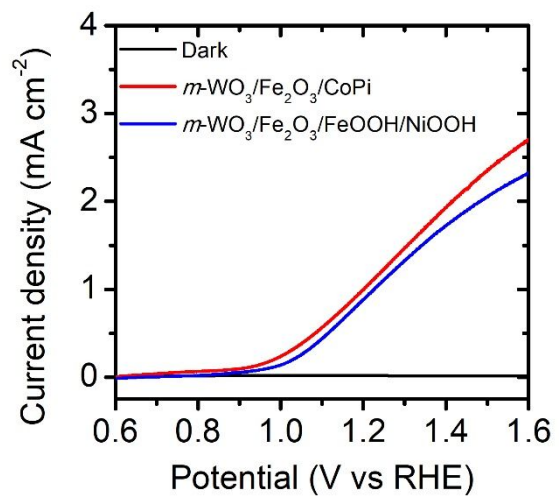


Figure S12. Photocurrent measurement of $m\text{-WO}_3/\text{Fe}_2\text{O}_3$ photoanodes with CoPi and FeOOH/NiOOH deposition.

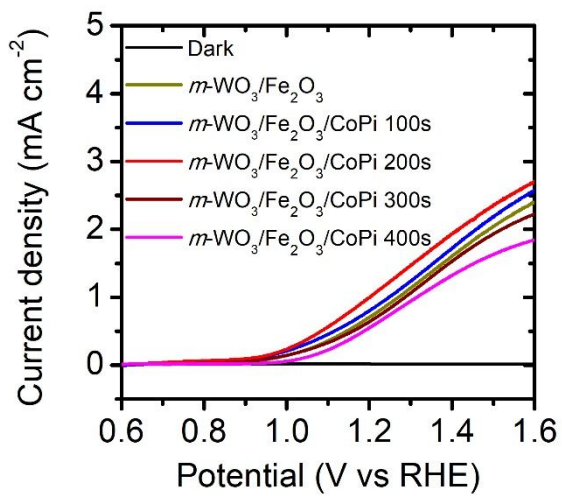


Figure S13. Photocurrent measurement of $m\text{-WO}_3/\text{Fe}_2\text{O}_3$ photoanode after Co-Pi co-catalyst deposition with different deposition times. After 200 seconds CoPi deposition, the photoanode showed 1.15 mA/cm^2 of photocurrent density, which is 1.4 times higher photocurrent at 1.23V vs RHE compared to the bare $m\text{-WO}_3/\text{Fe}_2\text{O}_3$ photoanode sample.

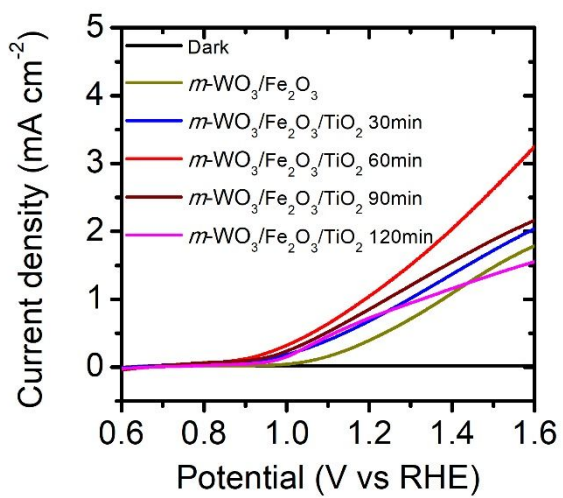


Figure S14. Photocurrent measurement of $m\text{-WO}_3/\text{Fe}_2\text{O}_3$ photoanode after TiO_2 overlayer deposition with different deposition time. After 60 minutes of deposition time, the photoanode showed 1.18 mA/cm^2 of photocurrent density at 1.23 V vs RHE .

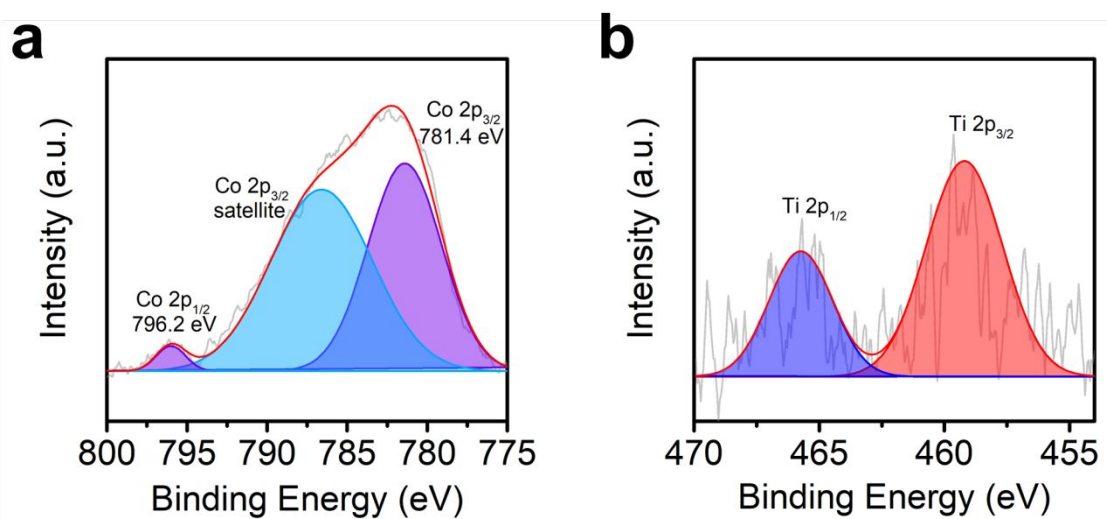


Figure S15. (a) Co 2p and (b) Ti 2p XPS spectra of *m*-WO₃/Fe₂O₃/TiO₂/CoPi photoanode

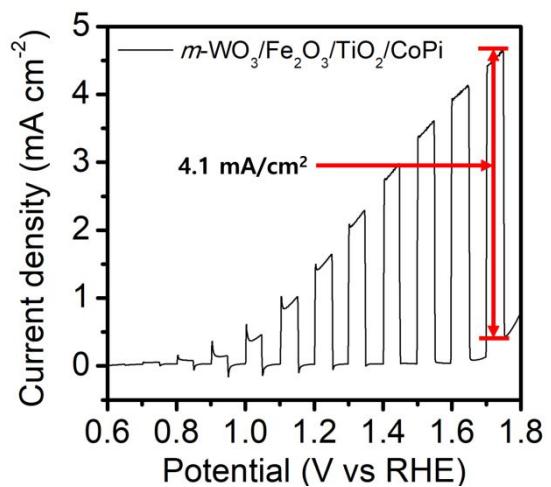


Figure S16. Photocurrent measurement of $m\text{-WO}_3/\text{Fe}_2\text{O}_3/\text{TiO}_2/\text{CoPi}$ photoanode under chopped light illumination. When the applied potential reached 1.7 V vs RHE, dark OER current is generated and the amount of current between photocurrent and dark current is considered as the practical maximum photocurrent density.

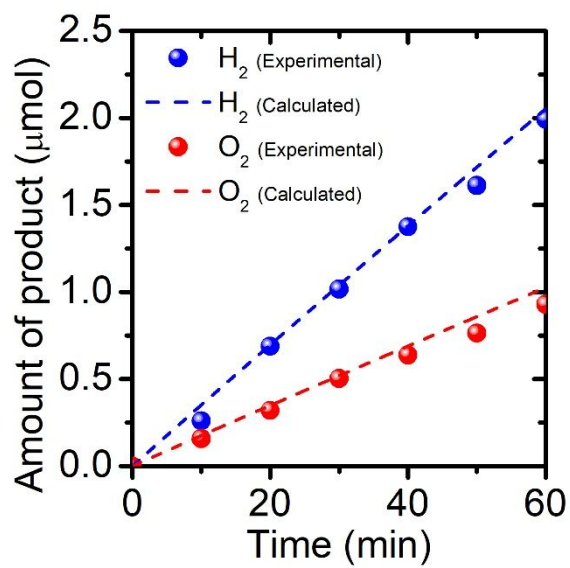


Figure S17. Comparison of theoretical and experimental amount of H_2 and O_2 produced from $m\text{-WO}_3/\text{Fe}_2\text{O}_3/\text{TiO}_2/\text{CoPi}$ photoanode.

References

- (1) Jin, T.; Diao, P.; Wu, Q.; Xu, D.; Hu, D.; Xie, Y.; Zhang, M. WO₃ nanoneedles/α-Fe₂O₃/cobalt phosphate composite photoanode for efficient photoelectrochemical water splitting. *Appl. Catal. B: Environ.* **2014**, 148-149, 304-310. DOI 10.1016/j.apcatb.2013.10.052.
- (2) Li, Y.; Feng, J.; Li, H.; Wei, X.; Wang, R.; Zhou, A. Photoelectrochemical splitting of natural seawater with α-Fe₂O₃/WO₃ nanorod arrays. *Int. J. Hydrogen Energy* **2016**, 41, 4096-4105. DOI 10.1016/j.ijhydene.2016.01.027.
- (3) Li, Y.; Zhang, L.; Liu, R.; Cao, Z.; Sun, X.; Liu, X.; Luo, J. WO₃@α-Fe₂O₃ Heterojunction Arrays with Improved Photoelectrochemical Behavior for Neutral pH Water Splitting. *ChemCatChem* **2016**, 8, 2765-2770. DOI 10.1002/cctc.201600475.
- (4) Davi, M.; Ogunu, G.; Schrader, F.; Rokicinska, A.; Kustrowski, P.; Slabon, A. Enhancing Photoelectrochemical Water Oxidation Efficiency of WO₃/α-Fe₂O₃ Heterojunction Photoanodes by Surface Functionalization with CoPd Nanocrystals. *Eur. J. Inorg. Chem.* **2017**, 2017, 4267-4274. DOI 10.1002/ejic.201700952.
- (5) Müller, A.; Kondofersky, I.; Folger, A.; Fattakhova-Rohlfing, D.; Bein T.; Scheu, C. Dual absorber Fe₂O₃/WO₃ host-guest architectures for improved charge generation and transfer in photoelectrochemical applications. *Mater. Res. Express* **2017**, 4, 016409. DOI 10.1088/2053-1591/aa570f.
- (6) Ng, K. H.; Minggu, L. J.; Mark-Leeb, W. F.; Arifina, K.; Jumalia, M. H. H.; Kassima, M. B. A new method for the fabrication of a bilayer WO₃/Fe₂O₃ photoelectrode for enhanced photoelectrochemical performance. *Mater. Res. Bull.* **2018**, 98, 47-52. DOI 10.1016/j.materresbull.2017.04.019.

- (7) Wu, Q.; Bu, Q.; Li, S.; Lin, Y.; Zou, X.; Wang, D.; Xie, T. Enhanced interface charge transfer via n-n $\text{WO}_3/\text{Ti-Fe}_2\text{O}_3$ heterojunction formation for water splitting. *J. Alloy. Compd.* **2019**, 803, 1105e1111. DOI 10.1016/j.jallcom.2019.06.371.
- (8) Zhang, J.; Zhu, G.; Liu, W.; Xi, Y.; Golosov, D. A.; Zavadski S. M.; Melnikov, S. N. 3D core-shell $\text{WO}_3@\alpha\text{-Fe}_2\text{O}_3$ photoanode modified by ultrathin FeOOH layer for enhanced photoelectrochemical performances. *J. Alloy. Compd.* **2020**, 834, 154992. DOI 10.1016/j.jallcom.2020.154992.
- (9) Zhang, Y.-F.; Zhu, Y.-K.; Lv, C.-X.; Lai, S.-J.; Xu, W.-J.; Sun, J.; Sun, Y.-Y.; Yang, D.-J. Enhanced visible-light photoelectrochemical performance via chemical vapor deposition of Fe_2O_3 on a WO_3 film to form a heterojunction. *Rare Met.* **2020**, 39, 841–849. DOI 10.1007/s12598-019-01311-5.